

Article

Selective Oxidation of Benzyl Alcohol by Ag/Pd/m-BiVO₄ Microspheres under Visible Light Irradiation

Xiujuan Yu ^{1,2}, Haiying Li ¹, Xueli Hao ¹, Zhiying Zhang ¹, Yan Wang ¹, Jingyi Li ^{1,*} and Kai Wang ²

¹ College of Chemistry and Chemical Engineering, Inner Mongolia University, Hohhot 010021, China; yuxiujuan810@163.com (X.Y.); lihaiying0528gsj@163.com (H.L.); hxl18747721020@163.com (X.H.); zhangzhiying2019@163.com (Z.Z.); wynmgny@163.com (Y.W.)

² Hebei Key Laboratory of Neuropharmacology, Hebei North University, Zhangjiakou 075000, China; bfxwangkai0313@163.com

* Correspondence: lijingyicn@163.com; Tel.: +86-1384-8129-221

Received: 26 January 2020; Accepted: 20 February 2020; Published: 22 February 2020



Abstract: A series of Ag/Pd/m-BiVO₄ (monoclinic) bimetallic photocatalytic materials with different loading amounts and different mass ratios of Ag and Pd were synthesized by a hydrothermal method and an NaBH₄ reduction method. The Ag/Pd/m-BiVO₄ photocatalyst with a total Ag and Pd loading of 2 wt% and an Ag-to-Pd mass ratio of 2:1 can selectively oxidize benzyl alcohol to benzaldehyde under visible light irradiation, the conversion rate was up to 89.9%, and the selectivity was greater than 99%. The conversion rate on Ag/Pd/m-BiVO₄ was higher than those on Ag/m-BiVO₄ and Pd/m-BiVO₄. The photocatalysts were characterized by X-ray powder diffraction (XRD), ultraviolet-visible diffuse reflection spectroscopy (UV-vis DRS), scanning electron microscopy (SEM), transmission electron microscopy (TEM), X-ray photoelectron spectroscopy (XPS), photoluminescence (PL) spectroscopy, N₂ adsorption-desorption isothermal curves (BET) and other means. The effects of different light wavelengths and light intensities were compared. Then, the effects of different alcohol derivatives on the reactions were explored. The cycle experiments proved that the Ag/Pd/m-BiVO₄ photocatalyst had good light stability and thermal stability. In addition, the capturing experiment of active species shows that the selective oxidation of benzyl alcohol is mainly accomplished through the synergistic action of h⁺, e⁻, •OH and •O₂⁻.

Keywords: Ag/Pd/m-BiVO₄; selective oxidation of benzyl alcohol; benzaldehyde; visible light irradiation

1. Introduction

Photocatalytic technology is a new technology that directly uses semiconductor materials and converts solar energy into chemical energy, which is an effective way to solve the current energy and environmental problems [1,2]. Photocatalytic technology is mainly applied to the degradation of organic pollutants, water decomposition and organic synthesis [3–5]. Compared with traditional methods, photocatalytic technology is characterized by mild conditions, green environmental protection, sustainable utilization and good development prospects [6,7]. Photocatalytic technology involves an oxidation-reduction reaction initiated by electrons and holes excited by semiconductor materials under illumination. Therefore, the photochemical conversion efficiency and the performance of semiconductor photocatalysts mainly depend on the light absorption capacity of these catalysts and the separation rate of photogenerated electrons and holes [8,9].

BiVO_4 is a light-yellow pigment with a bright color. Due to its advantages, such as a wide source of constituent elements, good chemical and thermal stability, innocuity, environmental friendliness and, in particular, its narrow forbidden band width and suitable valence band position, BiVO_4 has excellent photocatalytic activity [10–12]. BiVO_4 has three main crystal forms: monoclinic scheelite (m-s), tetragonal scheelite (t-s) and tetragonal zircon (t-z). The monoclinic scheelite phase has a narrow band gap energy (2.4 eV), is responsive to ultraviolet light and visible light and exhibits good photocatalytic activity [13,14]. However, pure BiVO_4 has limitations: photogenerated electrons are not easy to migrate and easily recombine with holes. This leads to a decrease in the activity upon visible light irradiation, which severely limits the photocatalytic performance of BiVO_4 [15,16]. To improve the photocatalytic activity of the BiVO_4 material, researchers have carried out a large number of modification studies on BiVO_4 in recent years [17–20]. One of the most commonly used methods to improve photocatalytic performance is to dope metals. When noble metals are loaded, the electron distribution of the BiVO_4 system is affected by the noble metals, and the surface properties change, thus improving the photocatalytic activity. Generally, the Fermi level of BiVO_4 is higher than that of the noble metals, and electrons will migrate from the semiconductor to the noble metals. When the Fermi levels of the noble metals and the semiconductor are equal, a Schottky barrier will be formed. A Schottky barrier can capture electrons and then decrease the recombination rate of the photogenerated carrier pairs [21,22]. Common noble metal loadings include Pt [23], Au [24], Pd [25] and Ag [26].

As carbonyl compounds are widely used in the food, medical, chemical and other industries, selective oxidation of alcohol compounds to aldehyde compounds is an important organic transformation [27]. In this paper, Ag/Pd/m- BiVO_4 nano-microspheres were prepared by a hydrothermal method and a NaBH_4 reduction method and exhibited good photocatalytic activity under visible light, far higher than that of pure m- BiVO_4 . Due to the surface plasmon resonance (SPR) effect of Ag in the Ag/Pd/m- BiVO_4 composite, Pd has a strong hydrogen absorption capacity, while the synergistic effect between different metals can change the catalytic performance [28,29]. In addition, because the electronegativity of Ag is stronger than that of Pd, when Ag is deposited on Pd nanoparticles, the catalytic efficiency of Pd in the selective oxidation of benzyl alcohol can be greatly improved. The bimetallic structure not only improves the catalytic activity but also reduces the amount of Pd used and enhances the stability [30].

2. Results and Discussion

A series of Ag/Pd/m- BiVO_4 bimetallic photocatalytic materials with different loading amounts and different mass ratios of Ag and Pd were synthesized; Ag/m- BiVO_4 and Pd/m- BiVO_4 monometallic photocatalytic materials with different loading amounts were also synthesized.

2.1. XRD Analysis

Figure 1 shows the XRD patterns of the different catalysts, in which the main peaks for the pure m- BiVO_4 nanospheres can be observed, such as (110), (011), (121), (040), (200), (002), (161) and other characteristic peaks, which are consistent with the standard card of m- BiVO_4 (JCPDS No. 14-0688) [31]. This shows that monoclinic scheelite phase m- BiVO_4 has been successfully prepared, and the XRD pattern of the composite material Ag/Pd/m- BiVO_4 is very similar to that of pure m- BiVO_4 . No obvious peaks of Ag and Pd were detected, which may be due to the smaller loading of noble metals and the smaller metal particles. This result also shows that the original crystal structure of m- BiVO_4 will not be destroyed during the loading process. At the same time, no other crystal phases are generated, indicating that no impurities are generated during the loading process.

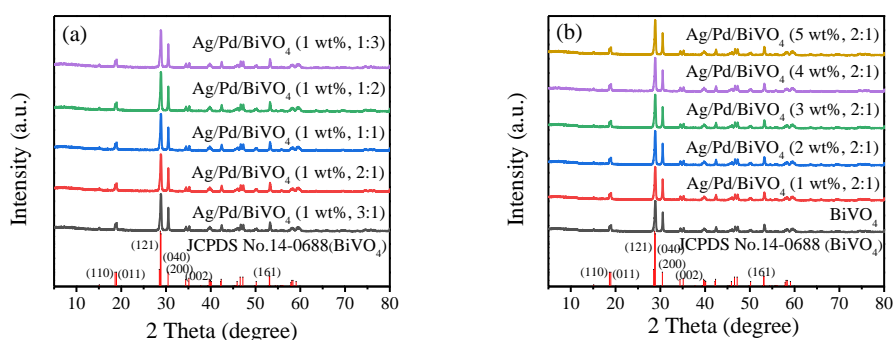


Figure 1. XRD patterns of the different catalysts. (a) catalysts of the different mass ratios of Ag and Pd, (b) catalysts of the different amounts of Ag and Pd.

2.2. SEM Analysis

Figure 2 shows SEM images of the prepared catalysts that was used to characterize the morphology of the materials. It can be seen from Figure 2a, b that m-BiVO₄ has a nano-microsphere structure with concave-convex structures on the surface. Figure 2c, d show SEM images of Ag/Pd/m-BiVO₄ (2 wt%, 2:1). The overall structure of the composite nano-microspheres has not changed, except that the concave-convex structures on the surface are covered with granular metals. Figure 2e shows an element plane distribution map for Ag/Pd/m-BiVO₄ (2 wt%, 2:1), showing the existence of Bi, V, and O and a uniform distribution of Ag and Pd nanoparticles on the surface.

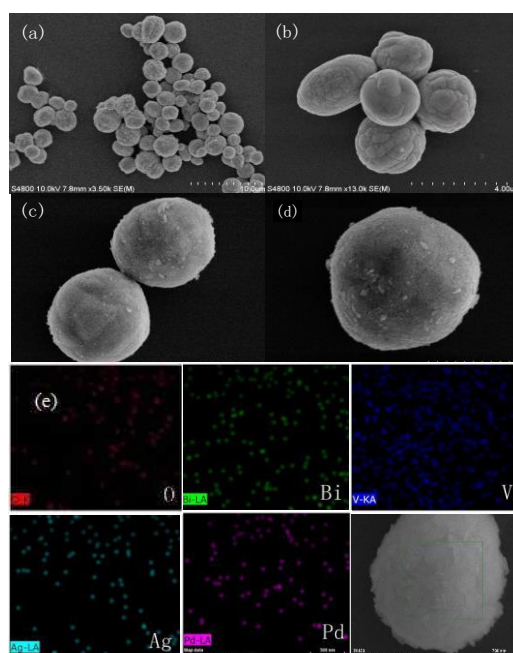


Figure 2. SEM images of different catalysts: (a,b) m-BiVO₄, (c,d) Ag/Pd/m-BiVO₄ (2 wt%, 2:1) and (e) Ag/Pd/m-BiVO₄ (2 wt%, 2:1) element plane distribution map.

2.3. TEM Analysis

Figure 3 shows TEM images of the prepared m-BiVO₄ and Ag/Pd/m-BiVO₄ (2 wt%, 2:1) composite nanospheres. From Figure 3a, the spherical structure of the material can be observed, and from Figure 3b,c, the existence and good dispersibility of Ag and Pd particles on the surface of the nanospheres can be observed. Figure 3d shows an HRTEM diagram of Ag/Pd/m-BiVO₄ (2 wt%, 2:1), in which lattice spacings of 0.308 nm, 0.219 nm and 0.237 nm can be observed, corresponding to the (121), (111) and (111) crystal surfaces of m-BiVO₄, Pd and Ag [30]. Figure 3e shows the EDX spectrum

of Ag/Pd/m-BiVO₄ (2 wt%, 2:1), which is basically consistent with the actual content of each element in the material.

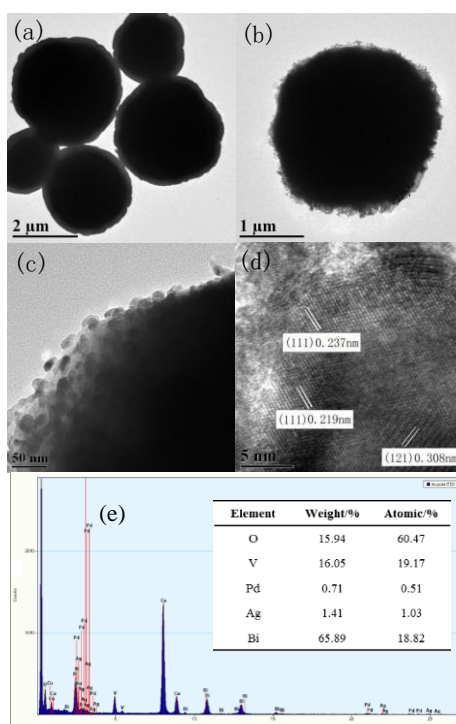


Figure 3. TEM images of the different catalysts: (a) m-BiVO₄, (b,c) Ag/Pd/m-BiVO₄ (2 wt%, 2:1), (d) HRTEM map of Ag/Pd/m-BiVO₄(2 wt%, 2:1) and (e) EDX map of Ag/Pd/m-BiVO₄ (2 wt%, 2:1).

2.4. UV-vis DRS Analysis

Figure 4a, b show UV-vis DRS diagrams of pure m-BiVO₄ and Ag/Pd/m-BiVO₄ with different mass ratios and with different loading amounts. From the diagram, it can be seen that the absorption edges of all test samples are approximately 500 nm [15], indicating that m-BiVO₄ absorbs in the visible region; Figure 4a shows that among the catalysts with different mass ratios, Ag/Pd/m-BiVO₄ (1 wt%, 2:1) has the strongest capacity to absorb visible light. As seen from the UV-vis DRS diagram of catalysts with different loading amounts in Figure 4b, Ag/Pd/m-BiVO₄ (2 wt%, 2:1) strongly absorbed visible light, which may be related to the synergy between the carrier and the precious metal. Figure 4c shows the band gap energy (E_g) spectra of m-BiVO₄ and Ag/Pd/m-BiVO₄ (2 wt%, 2:1). The E_g of these samples can be calculated based on the UV-vis absorption spectra data by using the equation $\alpha h\nu = A(h\nu - E_g)^{n/2}$, where α , h , ν , A and E_g represent the absorption coefficient, Planck's constant, the frequency, a constant and the optical band gap energy, respectively [11]. The value of n depends on the type of optical transition of the semiconductor. As a direct transition semiconductor, m-BiVO₄ has an n value of 1. The E_g values of the two catalysts are approximately 2.40 eV and 2.17 eV, respectively. When Ag and Pd are loaded on the surface of m-BiVO₄, the band gap of the prepared composite becomes narrower, thus increasing the visible light response of the prepared sample [12,32].

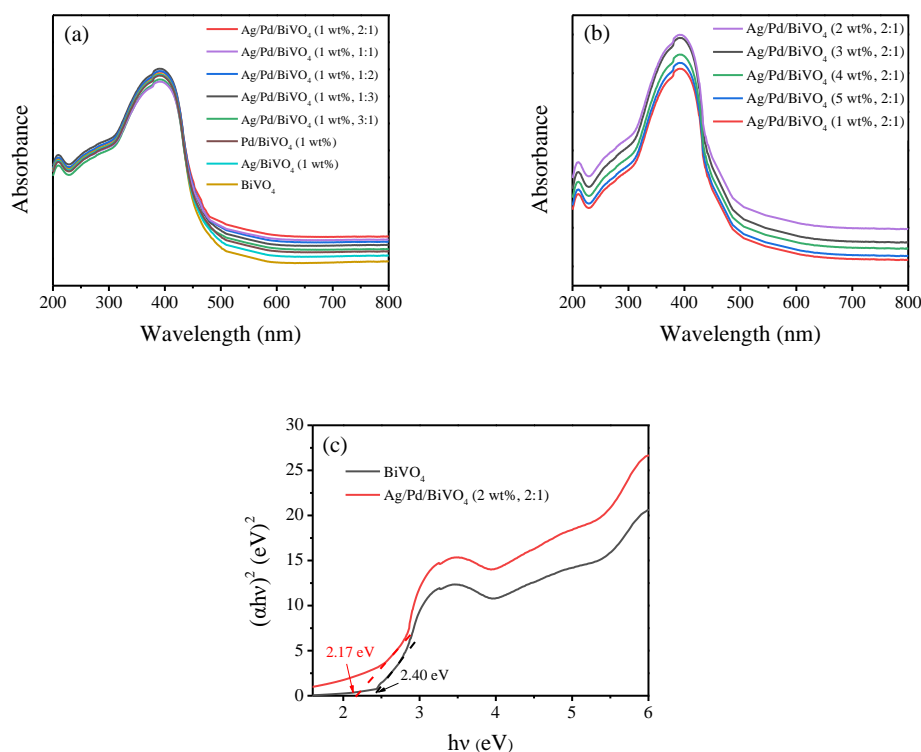


Figure 4. (a,b) UV-vis DRS pattern of different catalysts, and (c) the relative band gap energy of different catalysts.

2.5. XPS Analysis

Figure 5b–f show the XPS analysis of Bi 4f, V 2p, O 1s, Pd 3d and Ag 3d. The binding energy and element composition of Ag/Pd/m-BiVO₄ (2 wt%, 2:1) nanocomposites were studied. As shown in Figure 5a, the results show that the main components of the prepared sample are Bi, V, O, Pd and Ag. Figure 5b shows the 4f high-resolution XPS spectrum of Bi. It can be seen from the spectrum that the characteristic peaks at 158.5 eV and 163.8 eV correspond to the binding energies of Bi 4f_{7/2} and Bi 4f_{5/2}, respectively. Figure 5c shows a high-resolution XPS spectrum of V 2p, in which the main peaks at 516.0 eV and 523.5 eV correspond to V 2p_{3/2} and V 2p_{1/2}. Figure 5d shows a high-resolution XPS spectrum of O 1s, which can be divided into three peaks of 529.2 eV, 531.5 eV and 533.1 eV, with the main peak at 529.2 eV corresponding to the lattice oxygen of Bi₂O₂²⁺, the main peak at 531.5 eV corresponding to the acidic oxygen of VO₄²⁻ and the 533.1 eV peak corresponding to hydroxyl groups on the sample surface or H₂O adsorbed on the surface [21]. Figure 5e shows a 3d high-resolution XPS spectrum of Pd, in which the main peaks at 334.5 eV and 339.9 eV are attributed to Pd 3d_{5/2} and Pd 3d_{3/2}, which correspond to the zero valence binding energy of the metal state of Pd. Figure 5f shows two characteristic peaks at 367.2 eV and 373.2 eV are attributed to Ag 3d_{5/2} and Ag 3d_{3/2}, which correspond to the zero valence binding energy of the metal state of Ag [30,33]. The experimental results show that Ag and Pd are successfully loaded on the surface of m-BiVO₄ in the form of metals.

Figure S1 shows the XPS analysis of Bi 4f, V 2p, O 1s, and Pd 3d. The binding energy and element composition of Pd/m-BiVO₄ (2 wt%) nanocomposites were studied. As shown in Figure S1a, the results show that the main components of the prepared sample are Bi, V, O, and Pd. Figure S1b shows the 4f high-resolution XPS spectrum of Bi. It can be seen from the spectrum that the characteristic peaks at 158.6 eV and 163.9 eV correspond to the binding energies of Bi 4f_{7/2} and Bi 4f_{5/2}, respectively. Figure S1c shows a high-resolution XPS spectrum of V 2p, in which the main peaks at 516.1 eV and 523.7 eV correspond to V 2p_{3/2} and V 2p_{1/2}. Figure S1d shows a high-resolution XPS spectrum of O 1s, which can be divided into three peaks of 529.3 eV, 531.5 eV and 533.1 eV, with the main peak at 529.3 eV corresponding to the lattice oxygen of Bi₂O₂²⁺, the main peak at 531.5 eV corresponding to the acidic

oxygen of VO_4^{2-} and the 533.1 eV peak corresponding to hydroxyl groups on the sample surface or H_2O adsorbed on the surface [21]. Figure S1e shows a 3d high-resolution XPS spectrum of Pd, in which the main peaks at 334.7 eV and 334.1 eV are attributed to Pd $3d_{5/2}$ and Pd $3d_{3/2}$, which correspond to the zero valence binding energy of the metal state of Pd [30,33]. The experimental results show that Pd is successfully loaded on the surface of m-BiVO₄ in the form of metals. The comparison between the XPS results of Pd/m-BiVO₄ (2 wt%) and the XPS results of Ag/Pd/m-BiVO₄ (2 wt%, 2:1) in Figure 5 shows that the binding energies of the elements of monometallic material Pd/m-BiVO₄ (2 wt%) and bimetallic material Ag/Pd/m-BiVO₄ (2 wt%, 2:1) have slight change, which also proves that bimetallic material Ag/Pd/m-BiVO₄ (2 wt%, 2:1) has been successfully prepared.

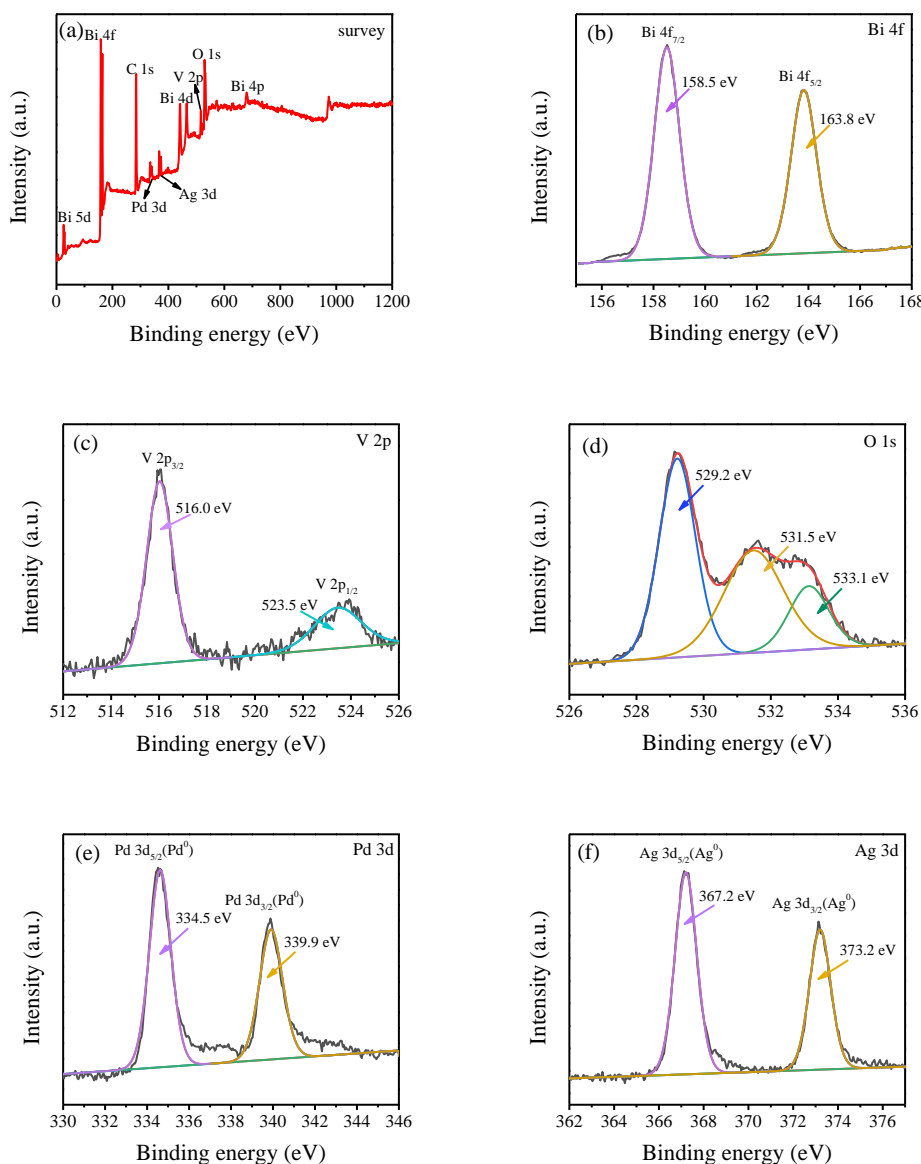


Figure 5. XPS spectra: (a) full spectrum of Ag/Pd/m-BiVO₄ (2 wt%, 2:1), (b) Bi 4f, (c) V 2p, (d) O 1s, (e) Pd 3d and (f) Ag 3d.

2.6. PL Analysis

Photoluminescence (PL) spectra are often used to study the excitation and transfer of photogenerated carriers in photocatalytic semiconductor materials. When the PL signal is low, the separation rate of photogenerated electron and hole pairs is high. The excitation wavelength of the

materials tested in Figure 6 is 320 nm. Ag/Pd/m-BiVO₄ (2 wt%, 2:1) nanocomposite has the lowest PL signal. The results show that the recombination rate of photoinduced electron and hole pairs can be effectively inhibited by modifying Ag and Pd on the surfaces of m-BiVO₄ nanospheres.

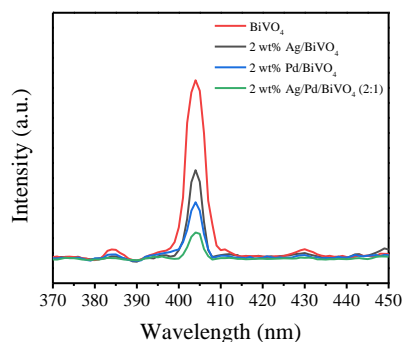


Figure 6. PL spectra of the different catalysts.

2.7. BET Analysis

To explain the increase in the specific surface area of the Ag/Pd/m-BiVO₄ (2 wt%, 2:1) composite, adsorption-desorption experiments and pore volume experiments on N₂ surfaces of the m-BiVO₄ and Ag/Pd/m-BiVO₄ (2 wt%, 2:1) catalysts were carried out, as shown in Figure 7. The results show that the N₂ adsorption and desorption curves of the tested samples are similar. The maximum pore volumes correspond to the pore diameters being approximately 360 and 400 nm for the m-BiVO₄ and Ag/Pd/m-BiVO₄ (2 wt%, 2:1) nanocomposites. The specific surface area of pure m-BiVO₄ is 16.14 m²g⁻¹, while that of Ag/Pd/m-BiVO₄ (2 wt%, 2:1) is increased to 22.26 m²g⁻¹. Therefore, Ag/Pd/m-BiVO₄ (2 wt%, 2:1) nanocomposite can provide more reactive sites.

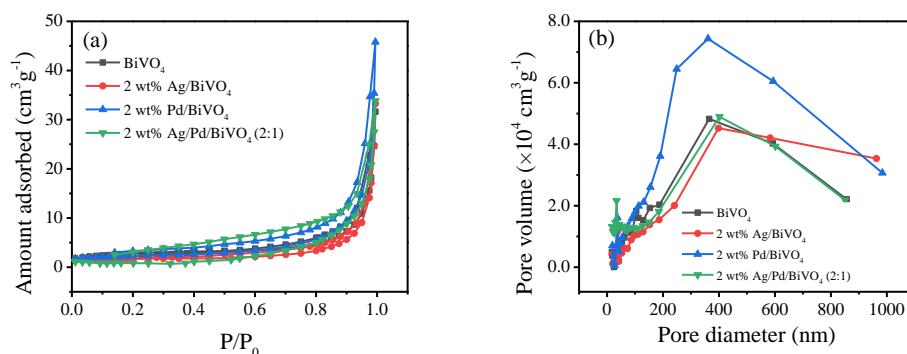
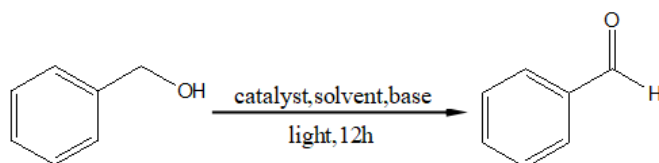


Figure 7. (a) N₂ adsorption/desorption isotherms of the different catalysts, and (b) the corresponding pore size distribution of the different catalysts.

2.8. Catalytic Activity

The reaction formula for the selective oxidation of benzyl alcohol to benzaldehyde is shown as follows:



The activities of the catalysts were tested in a photochemical reaction box. The selective oxidation of benzyl alcohol into benzaldehyde was carried out continuously for 12 h, including light reaction

and corresponding dark reaction experiments. The conversion rate and selectivity of the reactants and products were analyzed by GC. All the experiments are performed twice, and the average values are calculated.

Table 1 shows the effects of eight solvents with different polarities on the selective oxidation of benzyl alcohol. The reactions were carried out under a light source with an intensity of 3.0×10^{-2} W/cm². The reaction substrates included 50 mg of Ag/Pd/m-BiVO₄ (1 wt%, 1:1) catalyst, 1.0 mmol of KOH, 2 mmol of benzyl alcohol and 6 mL of solvent.

Table 1. Effect of different solvents on the selective oxidation of benzyl alcohol.

No.	Solvents	Polar Index	Light Irradiation		In Dark	
			Conv. (%)	Sel. (%)	Conv. (%)	Sel. (%)
1	DMF	6.4	30.1	>99	5.2	>99
2	1,4-Dioxane	4.8	61.4	>99	10.4	>99
3	Isopropanol	4.3	63.8	>99	10.5	>99
4	Toluene	2.4	70.7	>99	12.2	>99
5	n-heptane	0.2	51.2	92.1	8.6	90.4
6	Cyclohexane	0.1	40.7	88.0	8.2	87.7
7	n-Hexane	0.06	36.9	86.2	7.0	87.0
8	Petroleum ether	0.01	31.2	85.3	5.9	86.1

From the data in Table 1, it can be seen that the conversion rate and selectivity of the photoreactions are much higher than those of the dark reactions. With a decrease in the polarity of the solvent, the conversion rate of benzyl alcohol increased first and then decreased. When the polarity of the solvents was reduced to less than 0.2, the selectivity of benzaldehyde was reduced to less than 90%. When toluene was used as the solvent, the best conversion rate of benzyl alcohol was 70.7%, and the selectivity of benzaldehyde was over 99%.

Table 2 shows the effects of different types and amounts of alkali on the selective oxidation of benzyl alcohol. The reactions were carried out under a light source with an intensity of 3.0×10^{-2} W/cm². The reaction substrate included 50 mg of catalyst Ag/Pd/m-BiVO₄ (1 wt%, 1:1), 2 mmol of benzyl alcohol, 6 mL of toluene and a certain amount of base.

Table 2. Effect of different bases and the amount of base on the selective oxidation of benzyl alcohol.

No.	Bases	Light Irradiation		In Dark	
		Conv. (%)	Sel. (%)	Conv. (%)	Sel. (%)
1	1.0 mmol CH ₃ ONa	23.5	>99	3.4	>99
2	1.0 mmol Cs ₂ CO ₃	30.4	>99	3.6	>99
3	1.0 mmol K ₂ CO ₃	15.6	>99	2.4	>99
4	1.0 mmol Na ₂ CO ₃	26.1	>99	5.3	>99
5	1.0 mmol KOH	70.7	>99	12.2	>99
6	1.0 mmol LiOH	40.9	>99	10.4	>99
7	1.2 mmol NaOH	75.1	>99	13.3	>99
8	1.0 mmol NaOH	75.9	>99	13.1	>99
9	0.8 mmol NaOH	71.6	>99	13.0	>99
10	0.6 mmol NaOH	50.1	>99	12.1	>99
11	0.4 mmol NaOH	29.2	>99	7.6	>99
12	None	8.4	>99	0	>0

The experiment explored the influence of seven kinds of base with different strengths and amounts on the reactions. The conversion rate with a strong base was significantly higher than that with a weak base, and the conversion rate of the light reactions was much higher than that of the dark reactions. In this experiment, the base can neutralize part of H⁺ in the reaction environment, and the base can promote oxidation of hydroxyl hydrogen to aldehyde, thus promoting the progress of photocatalytic

reaction. When NaOH was selected as the reaction substrate, the conversion rate was the best, and the amount of NaOH used was optimized. The results showed that with increasing alkali content, the conversion first increased and then decreased. When the amount of NaOH added was 1.0 mmol, the conversion rate reached 75.9%, which may be due to the presence of excessive alkali occupying the active sites of the catalyst itself, thus affecting the reaction. The choice of base is based on specific experiments, including the choice of photocatalyst and the type of reactant as well as the specific environment of the reaction.

Table 3 shows the effects of different catalysts on the selective oxidation of benzyl alcohol. The reaction was carried out under a light source with an intensity of 3.0×10^{-2} W/cm². The reaction substrates included 50 mg of catalysts, 1.0 mmol of NaOH, 2 mmol of benzyl alcohol and 6 mL of toluene.

Table 3. Effect of different catalysts on the selective oxidation of benzyl alcohol.

No.	Catalysts	Light Irradiation		In Dark	
		Conv. (%)	Sel. (%)	Conv. (%)	Sel. (%)
1	BiVO ₄	30.7	>99	4.2	>99
2	Ag/BiVO ₄ (1wt%)	56.4	>99	6.9	>99
3	Pd/BiVO ₄ (1wt%)	65.8	>99	7.2	>99
4	Ag/Pd/BiVO ₄ (1wt%,3:1)	76.3	>99	9.8	>99
5	Ag/Pd/BiVO ₄ (1wt%,2:1)	79.8	>99	10.9	>99
6	Ag/Pd/BiVO ₄ (1wt%,1:1)	75.9	>99	13.1	>99
7	Ag/Pd/BiVO ₄ (1wt%,1:2)	72.7	>99	10.0	>99
8	Ag/Pd/BiVO ₄ (1wt%,1:3)	71.9	>99	10.4	>99
9	Ag/Pd/BiVO ₄ (2wt%,2:1)	89.9	>99	11.2	>99
10	Ag/Pd/BiVO ₄ (3wt%,2:1)	86.8	>99	10.7	>99
11	Ag/Pd/BiVO ₄ (4wt%,2:1)	83.1	>99	10.4	>99
12	Ag/Pd/BiVO ₄ (5wt%,2:1)	81.6	>99	10.2	>99

The conversion rate of m-BiVO₄ loaded with noble metal was higher than that of pure m-BiVO₄ under visible light irradiation, and the conversion rate of Ag and Pd bimetal loaded was higher than that of the catalysts loaded with single metal in Table 3. The conversion rate of benzyl alcohol on Ag/Pd/m-BiVO₄ (2 wt%, 2:1) was the best (89.9%). Both the loading ratio and the total loading amount of noble metals affect the conversion rate of the reaction, which may be determined by the interaction of metals and the relationship between the loading amount of noble metals and the specific surface area of the carrier m-BiVO₄.

Table 4 shows the effects of different catalyst dosages on the oxidation of benzyl alcohol. The reactions were carried out under a light source with an intensity of 3.0×10^{-2} W/cm². The reaction substrates included 1.0 mmol of NaOH, 2 mmol of benzyl alcohol, 6 mL of toluene and different amounts of Ag/Pd/m-BiVO₄ (2 wt%, 2:1) catalyst.

Table 4. Effect of the amount of catalyst on the selective oxidation of benzyl alcohol.

No.	Catalyst (mg)	Light Irradiation		In Dark	
		Conv. (%)	Sel. (%)	Conv. (%)	Sel. (%)
1	25	57.3	>99	8.4	>99
2	50	89.9	>99	11.2	>99
3	75	84.1	>99	11.9	>99
4	100	70.2	>99	12.1	>99

When the amount of catalyst added was 50 mg, the conversion rate was the best in Table 4. When the amount of catalyst used is small, it cannot generate enough photogenic charge carriers and cannot provide enough specific surface area, resulting in the lack of active substances and active sites

involved in the reaction. When the amount of catalyst used is large, a large amount of photocatalyst is suspended in the reaction liquid, which scatters the incident light, thus affecting the reaction [27].

Table 5 shows the effects of different illumination times on the selective oxidation of benzyl alcohol. The reaction was carried out under a light source with an intensity of 3.0×10^{-2} W/cm². The reaction substrates included 50 mg of Ag/Pd/m-BiVO₄ (2 wt%, 2:1) catalyst, 1.0 mmol of NaOH, 2 mmol of benzyl alcohol and 6 mL of toluene. With increasing illumination time, the conversion rate of benzyl alcohol increased. With an illumination time of more than 12 h, the conversion rate of benzyl alcohol increased slightly. Therefore, 12 h is the best illumination time.

Table 5. Effect of reaction time on the selective oxidation of benzyl alcohol.

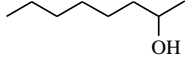
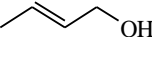
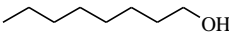
No.	Reaction Times (h)	Light Irradiation		In Dark	
		Conv. (%)	Sel. (%)	Conv. (%)	Sel. (%)
1	8	78.1	>99	10.7	>99
2	10	83.5	>99	12.2	>99
3	12	89.9	>99	11.2	>99
4	15	90.2	>99	13.3	>99
5	24	90.7	>99	13.9	>99

To study the selective oxidation of different alcohol derivatives by Ag/Pd/m-BiVO₄ (2 wt%, 2:1), 13 kinds of alcohol derivatives were selected. The reaction was carried out under a light source with an intensity of 3.0×10^{-2} W/cm². The reaction substrates included 50 mg of Ag/Pd/m-BiVO₄ (2 wt%, 2:1) catalyst, 1.0 mmol of NaOH, 2 mmol of alcohol derivatives and 6 mL of toluene. The results are shown in Table 6.

Table 6. Effect of alcohol derivatives on the selective oxidation of benzyl alcohol.

No.	R-CH ₂ -OH	Light Irradiation		In Dark	
		Conv. (%)	Sel. (%)	Conv. (%)	Sel. (%)
1		89.9	>99	11.2	>99
2		35.1	>99	10.7	>99
3		9.8	>99	3.1	>99
4		90.0	>99	13.5	>99
5		92.1	>99	13.8	>99
6		90.4	>99	13.6	>99
7		82.3	>99	20.6	>99
8		65.1	>99	21.9	>99

Table 6. Cont.

No.	R-CH ₂ -OH	Light Irradiation		In Dark	
		Conv. (%)	Sel. (%)	Conv. (%)	Sel. (%)
9		6.9	>99	0	0
10		3.7	>99	0	0
11		64.9	>99	23.9	>99
12		4.2	>99	1.0	>99
13		20.7	>99	7.3	>99

The catalyst has a poor catalytic effect on saturated aromatic alcohols or fatty alcohols with branched chain C, which may be because the hydroxyl hydrogen of such alcohols is not easy to separate. In addition, due to the large steric resistance of secondary aromatic alcohols or fatty alcohols, the catalytic effect of this catalyst on such alcohols is also not good. If an electron-donating group is attached to the para-position of a benzyl alcohol, the catalytic activity of the catalyst is not good, but if an electron-withdrawing group is attached to the para-position, the catalyst has good catalytic activity, which may be because the electron-donating group does not facilitate separation of the hydroxyl H.

In short, the Ag/Pd/m-BiVO₄ (2 wt%, 2:1) nanocomposite has strong catalytic activity for a class of aromatic alcohols with electron-withdrawing groups during the selective oxidation of alcohol derivatives to corresponding aldehydes and has poor catalytic activity for saturated fatty alcohols and secondary alcohols.

2.9. Effect of Light Intensity on The Selective Oxidation of Benzyl Alcohol

Figure 8 explores the influence of light intensity on the selective oxidation of benzyl alcohol. The light intensity has a great influence on the conversion rate of benzyl alcohol: with increasing light intensity, the conversion rate gradually increases.

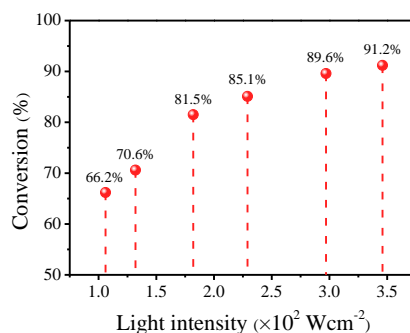


Figure 8. Effect of different light intensities on the selective oxidation of benzyl alcohol.

2.10. Effect of Light Wavelength on The Selective Oxidation of Benzyl Alcohol

Figure 9 explores the influence of light wavelength on the selective oxidation of benzyl alcohol when the above optimal conditions are selected. In the visible light range, the larger the wavelength range is, the higher the conversion rate of benzyl alcohol is. When the wavelength range is reduced to 510–800 nm, the conversion rate decreases obviously, which may be related to the light absorption range of Ag/Pd/m-BiVO₄ (2 wt%, 2:1) nano-microspheres in UV-vis DRS. The Ag/Pd/m-BiVO₄ (2 wt%, 2:1) composite has an obvious visible light absorption within 400–500 nm, which promoted the reaction. They are done by changing the filters in different wavelength ranges.

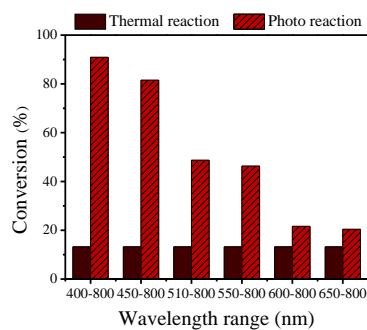


Figure 9. Effect of different light wavelengths on the selective oxidation of benzyl alcohol.

2.11. Cycle Capability Test of the Catalyst

To explore the stability of the photocatalyst, six cycles of experiments were carried out. The conversion rate changed little during the first three cycles, and the conversion rate decreased slightly after the fourth cycle. The prepared Ag/Pd/m-BiVO₄ (2 wt%, 2:1) nanospheres had good photostability and thermal stability, as shown in Figure 10.

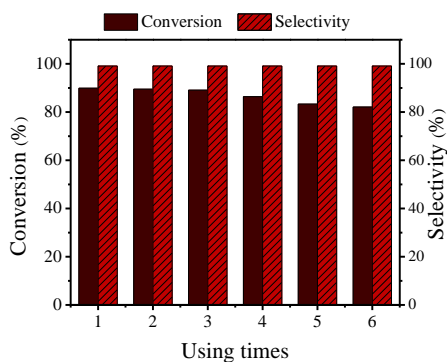


Figure 10. Recyclability test of the selective oxidation of benzyl alcohol.

2.12. Active Species Test

To explore the active species in the reaction, a capturing experiment of active species was carried out. With 2 mmol of benzyl alcohol as the reactant and 5 mmol of four quenchers, namely, ethylenediaminetetraacetic acid (EDTA), tert-butyl alcohol (t-BuOH), 1,4-benzoquinone (BQ) and carbon tetrachloride (CCl₄), were added as quenching agents for h⁺, •OH, •O₂⁻ and e⁻, respectively, the results are shown in Figure 11. The experimental results showed that the reaction quenching was the most obvious when EDTA was added, the conversion rate decreased significantly when BQ and CCl₄ were added, the conversion rate decreased slightly when t-BuOH was added. Therefore, the reaction was mainly completed through the synergistic effect of h⁺, e⁻, •OH and •O₂⁻.

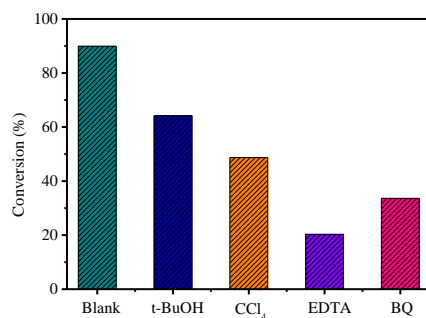


Figure 11. Capturing experiment of active species of Ag/Pd/m-BiVO₄ (2 wt%, 2:1).

3. Materials and Methods

3.1. Preparation of Photocatalysts

3.1.1. Preparation of m-BiVO₄

At room temperature, 5 mmol of Bi(NO₃)₃•5H₂O was dissolved in 30 mL of 0.2 M nitric acid, and magnetic stirring was performed to completely dissolve it to form liquid A. At the same time, 5 mmol of NH₄VO₃ was dissolved in 100 mL of deionized water and continuously stirred to completely dissolve it to form liquid B. Then, liquid A was slowly dropped into liquid B, the mixed liquid was fully stirred for approximately 30 min, the pH of the solution was adjusted to 6–7 (several pH ranges, including 2–3, 4–5, 8–9 and 10–11, were tested, and the optimal pH range was 6–7) with NH₃•H₂O, and then the mixed liquid was transferred to a 100 mL high-pressure reaction kettle, heated at 130 °C (several temperatures, including 100 °C, 150 °C and 180 °C, were tested, and the optimal temperature was 130 °C) for 15 h, cooled to room temperature, washed with deionized water and anhydrous ethanol to wash the precipitate, dried at 60 °C for 12 h, fully grinded to obtain m-BiVO₄ powder and dried for storage.

3.1.2. Preparation of Ag/Pd/m-BiVO₄

First, 2.0 g of the carrier m-BiVO₄ was accurately weighed and dissolved in 200 mL of deionized water; then, continuous ultrasound was carried out for 30 min and 0.1 g of PEG2000 was added. The mixture was stirred for 10 min, and ultrasound was carried out for 10 min. A pipette was used to measure a certain amount of PdCl₂ with an accurate concentration and drop it into the above solution slowly for approximately 20 min. Next, 10 mL of lysine (0.53 M) was accurately measured and added dropwise to the above solution over approximately 10 min, and the solution was stirred for 30 min. NaBH₄ (0.03 g) was dissolved in 2.5 mL of water, added dropwise into the above solution, and dried for approximately 10 min; then, 2.5 mL of HCl (0.3 M) was dropped into the above solution for approximately 10 min, and stirred for 1 h to form a Pd/m-BiVO₄ solution. A certain amount of AgCl solution with an accurate concentration was measured and dropped into the mixed solution slowly for approximately 20 min. Then, 20 mL of lysine (0.53 M) was accurately measured and added dropwise to the above solution over approximately 10 min, and the solution was stirred for 30 min. NaBH₄ (0.06 g) was dissolved in 5.0 mL of water and added dropwise into the above solution for approximately 10 min; then, 5.0 mL of HCl (0.3 M) was accurately measured and dripped into the above solution slowly for approximately 10 min, and the solution was stirred for 1 h to form a Ag/Pd/m-BiVO₄ solution, which was aged for 24 h, washed with deionized water and ethanol three times and dried at 60 °C for 12 h.

3.2. Characterization Methods

X-ray diffraction (XRD) was used to analyze the crystal phases of the materials. A Rigaku D/MAX-2500 X-ray diffractometer was used with Cu/Kα radiation ($\lambda = 1.5405$ nm), a voltage of 40 kV, and a current of 100 mA (Rigaku Industrial Corporation, Osaka, Japan).

Scanning electron microscopy (SEM, model S-4800, Hitachi Limited Company, Tokyo, Japan) was used to observe the morphological characteristics of the materials.

Transmission electron microscopy (TEM) and high-resolution transmission electron microscopy (HRTEM) images were obtained by using an F20 S-double electron microscope (Tecnai G2, FEI Company, Hillsborough, OR, USA) at an accelerating voltage of 200 kV.

The X-ray photoelectron spectra (XPS) of the prepared samples were measured using a Thermo Fisher ESCALAB 250Xi spectrometer equipped with an Al-Kα X-ray source ($h\nu = 1486.6$ eV) (Thermo Fisher Scientific Company, Waltham, MA, USA).

The UV-vis diffuse reflectance spectra (UV-vis-DRS) of the prepared samples were measured using a UV-vis spectrophotometer (U-3900, Hitachi Limited Company, Tokyo, Japan) equipped with an integrated sphere component based on 100% barium sulfate.

The photoluminescence (PL) spectra of the samples were measured by using an Edinburgh Instruments FLS920 fluorescence spectrometer (Edinburgh Instruments, Edinburgh, Scot., British). The light source used was a 450 W pulsed xenon lamp. The excitation wavelength was 320 nm, and the emission spectrum wavelength range was 370–450 nm.

The specific surface area and pore size distribution of the samples were measured by the multipoint Brunauer-Emmett-Teller (BET) method (Quantachrome Instruments, Corporate Headquarters, Boynton Beach, FL, USA).

The reaction products were quantitatively analyzed by gas chromatography (GC-2030, Shimadzu Company, Kyoto, Japan).

3.3. Photocatalytic Activity Analysis

The activities of the prepared photocatalysts were evaluated by selective oxidation of benzyl alcohol to benzaldehyde under visible light irradiation. The activities of the catalysts were tested in a photochemical reaction box (Beijing Zhongjiao Jinyuan Technology Co., Ltd., Beijing, China). The reaction tank was equipped with a xenon lamp ($P \leq 500$ W) with an adjustable power as the light source, an ultraviolet light cut-off filter ($\lambda > 400$ nm) and a circulating water cold trap. In the experiment, 50 mg of catalyst powder was dispersed in a quartz tube containing 2 mmol of benzyl alcohol in 6 mL of toluene solution. The strong alkali NaOH (1.0 mmol) was added to the mixed solution and stirred under visible light for 12 h. The reaction temperature was 15 ± 3 °C.

3.4. Recycling Test

Six cycle experiments were conducted on the Ag/Pd/m-BiVO₄ (2 wt%, 2:1) catalyst, a sufficient number of activity measurements were conducted in parallel experiments ($n = 50$), and the catalyst was recycled after the activity measurements and reused six times. After each experiment, the recovered catalyst was washed and dried, and the photocatalytic performance of the catalyst was analyzed six times.

4. Conclusions

Ag/Pd/m-BiVO₄ (2 wt%, 2:1) nanosphere composites were successfully prepared by the NaBH₄ reduction method with m-BiVO₄ as the carrier. The synergistic effect of bimetals improves the performance of the catalyst in the selective oxidation of benzyl alcohol and increases the separation efficiency of electrons and holes. Under the optimal reaction conditions, a mixture of 50 mg of Ag/Pd/m-BiVO₄ (2 wt%, 2:1), 1.0 mmol of NaOH, 2 mmol of benzyl alcohol and 6 mL of toluene was irradiated continuously for 12 h under a light source with an intensity of 3.0×10^{-2} W/cm², and the conversion rate reached 89.9%. Cyclic experiments confirmed that the catalyst had good photostability and thermal stability. Capturing experiments of active species showed that the reaction was mainly completed by the synergistic effect of h^+ , e^- , \bullet OH, and \bullet O₂⁻.

Supplementary Materials: The following are available online at <http://www.mdpi.com/2073-4344/10/2/266/s1>, Figure S1: XPS spectra: (a) full spectrum of Pd/m-BiVO₄ (2 wt%), (b) Bi 4f, (c) V 2p, (d) O 1s, (e) Pd 3d. Table S1: The composition of Ag-Pd of the catalysts.

Author Contributions: X.Y. prepared the different photocatalysts. X.Y. and H.L. tested the activity of different photocatalysts. The photocatalysts were characterized by X.H., Z.Z. and Y.W., K.W. did some ancillary work. The manuscript was drafted by X.Y. and J.L. All authors read and approved the final manuscript.

Funding: This work was financially supported by the National Natural Science Foundation of China (NSFC, Nos. 20567002 and 21067007), the Natural Science Fund of Inner Mongolia (2010MS0203 and 2014MS0201), the 2013 Annual Grassland Talents Project of Inner Mongolia Autonomous Region, the 2013 Annual Inner Mongolia

Talent Development Fund, the Natural College Student Innovation and Entrepreneurship Training (201810092007) and the College Student Innovation and Entrepreneurship Training (xj201964, Hebei Province).

Conflicts of Interest: The authors declare no conflicts of interest.

References

1. Wang, R.S.; Li, B.X.; Xiao, Y.; Tao, X.Q.; Su, X.T.; Dong, X.P. Optimizing Pd and Au-Pd decorated Bi₂WO₆ ultrathin nanosheets for photocatalytic selective oxidation of aromatic alcohols. *J. Catal.* **2018**, *364*, 154–165. [[CrossRef](#)]
2. Wang, J.Z.; Jin, J.; Wang, X.G.; Yang, S.N.; Zhao, Y.L.; Wu, Y.W.; Dong, S.Y.; Sun, J.Y.; Sun, J.H. Facile fabrication of novel BiVO₄/Bi₂S₃/MoS₂ n-p heterojunction with enhanced photocatalytic activities towards pollutant degradation under natural sunlight. *J. Colloid Interf. Sci.* **2017**, *505*, 805–815. [[CrossRef](#)] [[PubMed](#)]
3. You, Y.; Wang, S.B.; Xiao, K.; Ma, T.Y.; Zhang, Y.H.; Huang, H.W. Z-scheme g-C₃N₄/Bi₄NbO₈Cl heterojunction for enhanced photocatalytic hydrogen production. *ACS Sustain. Chem. Eng.* **2018**, *6*, 16219–16227. [[CrossRef](#)]
4. Jin, B.B.; Yao, G.D.; Wang, X.G.; Ding, K.F.; Jin, F.M. Photocatalytic oxidation of glucose into formate on nano TiO₂ catalyst. *ACS Sustain. Chem. Eng.* **2017**, *5*, 6377–6381. [[CrossRef](#)]
5. Babu, P.; Mohanty, S.; Naik, B.; Parida, K. Serendipitous assembly of mixed phase BiVO₄ on B-Doped g-C₃N₄: An appropriate p-n heterojunction for photocatalytic O₂ evolution and Cr (VI) reduction. *Inorg. Chem.* **2019**, *58*, 12480–12491. [[CrossRef](#)] [[PubMed](#)]
6. Samanta, S.; Khilari, S.; Pradhan, D.; Srivastava, R. An efficient, visible light driven, selective oxidation of aromatic alcohols and amines with O₂ using BiVO₄/g-C₃N₄ nanocomposite: A systematic and comprehensive study toward the development of a photocatalytic process. *ACS Sustain. Chem. Eng.* **2017**, *5*, 2562–2577. [[CrossRef](#)]
7. Chong, B.; Chen, L.; Wang, W.T.; Han, D.Z.; Wang, L.; Feng, L.J.; Li, Q.; Li, C.H. Visible-light-driven Ag-decorated g-C₃N₄/Bi₂WO₆ Z-scheme composite for high photocatalytic activity. *Mater. Lett.* **2017**, *204*, 149–153. [[CrossRef](#)]
8. Wang, J.J.; Tang, L.; Zeng, G.G.; Liu, Y.N.; Zhou, Y.Y.; Deng, Y.C.; Wang, J.J.; Peng, B. Plasmonic Bi metal deposition and g-C₃N₄ coating on Bi₂WO₆ microspheres for efficient visible-light photocatalysis. *ACS Sustain. Chem. Eng.* **2016**, *5*, 1062–1072. [[CrossRef](#)]
9. He, W.J.; Sun, Y.J.; Jiang, G.M.; Huang, H.W.; Zhang, X.M.; Dong, F. Activation of amorphous Bi₂WO₆ with synchronous Bi metal and Bi₂O₃ coupling: Photocatalysis mechanism and reaction pathway. *Appl. Catal. B Environ.* **2018**, *232*, 340–347. [[CrossRef](#)]
10. Song, J.; Seo, M.J.; Lee, T.H.; Jo, Y.R.; Lee, J.; Kim, T.L.; Kim, S.Y.; Kim, S.M.; Jeong, S.Y.; An, H.; et al. Tailoring crystallographic orientations to substantially enhance charge separation efficiency in anisotropic BiVO₄ photoanodes. *ACS Catal.* **2018**, *8*, 5952–5962. [[CrossRef](#)]
11. Jing, Q.F.; Feng, X.Y.; Zhao, X.J.; Duan, Z.Y.; Pan, J.L.; Chen, L.M.; Liu, Y.N. Bi/BiVO₄ chain-like hollow microstructures: Synthesis, characterization and application as visible-light-active photocatalysts. *ACS Appl. Nano Mater.* **2018**, *1*, 2653–2661. [[CrossRef](#)]
12. He, B.; Li, Z.P.; Zhao, D.; Liu, H.H.; Zhong, Y.J.; Ning, J.Q.; Zhang, Z.Y.; Wang, Y.J.; Hu, Y. Fabrication of porous Cu-doped BiVO₄ nanotubes as efficient oxygen-evolving photocatalysts. *ACS Appl. Nano Mater.* **2018**, *1*, 2589–2599. [[CrossRef](#)]
13. Dong, C.W.; Lu, S.Y.; Yao, S.Y.; Ge, R.; Wang, Z.D.; Wang, Z.; An, P.F.; Liu, Y.; Yang, B.; Zhang, H. Colloidal synthesis of ultrathin monoclinic BiVO₄ nanosheets for Z-scheme overall water splitting under visible light. *ACS Catal.* **2018**, *8*, 8649–8658. [[CrossRef](#)]
14. Sajid, M.M.; Khan, S.B.; Shad, N.A.; Amin, N.; Zhang, Z.J. Visible light assisted photocatalytic degradation of crystal violet dye and electrochemical detection of ascorbic acid using a BiVO₄/FeVO₄ heterojunction composite. *RSC Adv.* **2018**, *8*, 23489–23498. [[CrossRef](#)]
15. Grigioni, I.; Stamplecoskie, K.G.; Selli, E.; Kamat, P.V. Dynamics of photogenerated charge carriers in WO₃/BiVO₄ heterojunction photoanodes. *J. Phys. Chem. C.* **2015**, *119*, 20792–20800. [[CrossRef](#)]
16. Pan, Q.G.; Zhang, C.; Xiong, Y.J.; Mi, Q.X.; Li, D.D.; Zou, L.L.; Huang, Q.H.; Zou, Z.Q.; Yang, H. Boosting charge separation and transfer by plasmon-enhanced MoS₂/BiVO₄ p-n heterojunction composite for efficient photoelectrochemical water splitting. *ACS Sustain. Chem. Eng.* **2018**, *6*, 6378–6387. [[CrossRef](#)]

17. Zhang, L.Y.; Dai, Z.X.; Zheng, G.H.; Yao, Z.F.; Mu, J.J. Superior visible light photocatalytic performance of reticular BiVO₄ synthesized via a modified sol-gel method. *RSC Adv.* **2018**, *8*, 10654–10664. [[CrossRef](#)]
18. Chen, P.; Li, Y.Z.; Xiao, C.X.; Chen, L.; Guo, J.K.; Shen, S.; Au, C.T.; Yin, S.F. Preparation of helical BiVO₄/Ag/C₃N₄ for selective oxidation of C-H bond under visible light irradiation. *ACS Sustain. Chem. Eng.* **2019**, *7*, 17500–17506. [[CrossRef](#)]
19. Ni, S.N.; Zhou, T.T.; Zhang, H.N.; Cao, Y.Q.; Yang, P. BiOI/BiVO₄ two-dimensional hetero-nanostructures for visible-light photocatalytic degradation of rhodamine B. *ACS Appl. Nano Mater.* **2018**, *1*, 5128–5141. [[CrossRef](#)]
20. Zhao, Y.; Li, R.G.; Mu, L.C.; Li, C. The Significance of crystal morphology controlling in semiconductor-based photocatalysis: A case study on BiVO₄ photocatalyst. *Cryst. Growth Des.* **2017**, *17*, 2923–2928. [[CrossRef](#)]
21. Zhao, W.; Feng, Y.; Zhang, J.; Zhu, F.X.; Sheng, Z.H.; Dai, B.L.; Dennis, Y.C.L.; Zhang, L.L.; Xu, J.M. A novel Ag/p-AgBr/n-BiVO₄ plasmonic heterojunction photocatalyst: Study on the excellent photocatalytic performance and photocatalytic mechanism. *ACS Appl. Energy Mater.* **2018**, *2*, 694–704.
22. Tao, X.Q.; Shao, L.Z.; Wang, R.S.; Xiang, H.P.; Li, B.X. Synthesis of BiVO₄ nanoflakes decorated with AuPd nanoparticles as selective oxidation photocatalysts. *J. Colloid Interf. sci.* **2019**, *541*, 300–311. [[CrossRef](#)] [[PubMed](#)]
23. Pan, X.Y.; Chen, X.X.; Yi, Z.G. Defective, porous TiO₂ nanosheets with Pt decoration as an efficient photocatalyst for ethylene oxidation synthesized by a C₃N₄ templating method. *ACS Appl. Mater. Interf.* **2016**, *8*, 10104–10108. [[CrossRef](#)] [[PubMed](#)]
24. Zhao, H.L.; Zheng, X.Y.; Feng, X.H.; Li, Y. CO₂ reduction by plasmonic Au nanoparticles decorated TiO₂ photocatalyst with an ultrathin Al₂O₃ interlayer. *J. Phys. Chem. C.* **2018**, *122*, 18949–18956. [[CrossRef](#)]
25. Sharma, M.; Das, B.; Sharma, M.; Deka, B.K.; Park, Y.B.; Bhargava, S.K.; Bania, K.K. Pd/Cu-oxide nanoconjugate at zeolite-Y crystallite crafting the mesoporous channels for selective oxidation of benzyl-alcohols. *ACS Appl. Mater. Interf.* **2017**, *9*, 35453–35462. [[CrossRef](#)] [[PubMed](#)]
26. Luo, B.F.; Xu, D.B.; Li, D.; Wu, G.L.; Wu, M.M.; Shi, W.D.; Chen, M. Fabrication of a Ag/Bi₃TaO₇ plasmonic photocatalyst with enhanced photocatalytic activity for degradation tetracycline. *ACS Appl. Mater. Interf.* **2015**, *7*, 17061–17069. [[CrossRef](#)] [[PubMed](#)]
27. She, H.D.; Zhou, H.; Li, L.S.; Wang, L.; Huang, J.W.; Wang, Q.Z. Nickel-doped excess oxygen defect titanium dioxide for efficient selective photocatalytic oxidation of benzyl alcohol. *ACS Sustain. Chem. Eng.* **2018**, *6*, 11939–11948. [[CrossRef](#)]
28. Hayashido, Y.; Naya, S.I.; Tada, H. Local electric field-enhanced plasmonic photocatalyst: Formation of Ag cluster-incorporated AgBr nanoparticles on TiO₂. *J. Phys. Chem. C.* **2016**, *120*, 19663–19669. [[CrossRef](#)]
29. Su, R.; Dimitratos, N.; Liu, J.J.; Carter, E.; Althahban, S.; Wang, X.Q.; Shen, Y.B.; Wendt, S.; Wen, X.D.; Niemantsverdriet, J.W.; et al. Mechanistic insight into the interaction between a titanium dioxide photocatalyst and Pd cocatalyst for improved photocatalytic performance. *ACS Catal.* **2016**, *6*, 4239–4247. [[CrossRef](#)]
30. Liu, H.X.; Wang, M.; Zhang, X.Q.; Ma, J.T.; Lu, G.X. High efficient photocatalytic hydrogen evolution from formaldehyde over sensitized Ag@Ag-Pd alloy catalyst under visible light irradiation. *Appl. Catal. B Environ.* **2018**, *237*, 563–573. [[CrossRef](#)]
31. Wang, W.Z.; Huang, X.W.; Wu, S.; Zhou, Y.X.; Wang, L.J.; Shi, H.L.; Liang, Y.J.; Zou, B. Preparation of p-n junction Cu₂O/BiVO₄ heterogeneous nanostructures with enhanced visible-light photocatalytic activity. *Appl. Catal. B Environ.* **2013**, *134*, 293–301. [[CrossRef](#)]
32. Deng, Y.C.; Tang, L.; Zeng, G.G.; Feng, C.Y.; Dong, H.R.; Wang, J.J.; Feng, H.P.; Liu, Y.N.; Zhou, Y.Y.; Pang, Y. Plasmonic resonance excited dual Z-scheme BiVO₄/Ag/Cu₂O nanocomposite: Synthesis and mechanism for enhanced photocatalytic performance in recalcitrant antibiotic degradation. *Environ. Sci. Nano* **2017**, *4*, 1494–1511. [[CrossRef](#)]
33. Gao, J.; Si, Z.C.; Xu, Y.F.; Liu, L.P.; Zhang, Y.Y.; Wu, X.D.; Ran, R.; Weng, D. Pd-Ag@CeO₂ catalyst of core-shell structure for low temperature oxidation of toluene under visible light irradiation. *J. Phys. Chem. C.* **2018**, *123*, 1761–1769. [[CrossRef](#)]

